J Elasticity (2006) 85: 153–173
DOI 10.1007/s10659-006-9076-y

On the Size of RVE in Finite Elasticity of Random Composites

Z. F. Khisaeva · M. Ostoja-Starzewski

Received: 5 April 2006 / Accepted: 16 June 2006 /
Published online: 30 August 2006

Abstract This paper presents a quantitative study of the size of representative volume element (RVE) of random matrix-inclusion composites based on a scale-dependent homogenization method. In particular, mesoscale bounds defined under essential or natural boundary conditions are computed for several nonlinear elastic, planar composites, in which the matrix and inclusions differ not only in their material parameters but also in their strain energy function representations. Various combinations of matrix and inclusion phases described by either a neo-Hookean or Ogden function are examined, and these are compared to those of linear elastic types.

Key words random composites · representative volume element · mesoscale bounds · homogenization theory · micromechanics · finite elasticity

Mathematics Subject Classifications (2000) 74A40 · 74B20 · 74Q20

1 Introduction

Random composites constitute an important group of natural (especially, biological) as well as man-made modern materials. Such materials generally consist of fibres, particles, nanoclusters, or grains randomly distributed in a solid matrix. The compelling questions arising when dealing with such microstructures are: What are the effective properties of the composite? Is it possible to predict the overall response of the material, knowing the properties of its constituents? How large is the size of the representative volume element (RVE) to represent the entire microstructure?

Consider three length scales: the heterogeneity size d (e.g., dispersion, void, single grain); the size L_{RVE} of the mesoscale or the representative volume element (RVE), at which the composite appears to be a representative of the entire ensemble; the macroscale

Z. F. Khisaeva (✉)
Department of Mechanical Engineering, McGill University, Montréal, QC H3A 2K6, Canada
e-mail: zemfira.khisaeva@mcgill.ca

M. Ostoja-Starzewski
Department of Mechanical Science and Engineering, University of Illinois at Urbana-Champaign, Urbana, IL 61801, USA

L_{macro} (the size of the body). These three scales are related to each other through the inequalities

$$d < L_{\text{RVE}} \leq L_{\text{macro}}, \tag{1}$$

also called a *separation of scales*, and commonly taken for granted in the homogenization theory. The mesoscale links microscopic properties with the macroscopic behaviour and is a convenient, intermediate scale to work with. In the absence of spatial periodicity in the random microstructure, the RVE is achieved exactly only in the limiting case of $\delta \to \infty$, where $\delta = L/d$ is a non-dimensional measure of the scale size.

In many cases, however, one does not need to consider infinitely large domains for the determination of material properties, as these can be attained with a sufficient accuracy on a finite scale. This scale (or the size of the RVE) has been a question of considerable attention in the past decade. In the context of small deformation theory the advances in these area are due to the work by Huet [1], Sab [2], Hazanov and Huet [3], Drugan and Willis [4], Gusev [5], Moulinec and Suquet [6], Hazanov [7], Michel et al. [8], Drugan [9], Zohdi and Wriggers [10, 11], Segurado and Llorka [12], Ren and Zheng [13], Soize [14], Lachihab and Sab [15], Sab and Nedjar [16], Ostoja-Starzewski [17], see also references therein.

Nonlinear composites in the setting of finite elasticity have not been researched as extensively as linear elastic materials due to the obvious reason of complexity of the problem. The influence of the number of particles on the effective stress response of the composite subjected to finite deformations was studied numerically by Löhnert and Wriggers [18] and Löhnert [19]. Hohe and Becker [20] performed numerical homogenization of a periodic polymeric foams at finite strain. Second order homogenization scheme was considered by Kouznetsova et al. [21].

The present study is concerned with an alternative approach to the determination of RVE properties and the RVE size. As δ increases, the material properties approach effective values with a certain rate that depends on the composite microstructure, properties' mismatch of the constituents, their interaction on a microscale, the physics of the problem (either elastic or plastic, etc.), the setting in 2-D (two-dimensional) or 3-D [17, 22]. In this paper we quantitatively investigate the convergence trend (i.e., scale effects) in the stochastic constitutive law of random composites, whose constitutive equations are nonlinear elastic and large deformations are involved. Investigations of such a trend allow to estimate the size of the RVE with a known error, and it is up to an engineer to decide how large an error can be acceptable for a certain engineering application. In effect, the present paper reports a computation of recently derived mesoscale upper and lower bounds (based on uniform kinematic and static boundary conditions, respectively) for nonlinear elastic, random composites at finite strains [23]. We compute such bounds for composites of several different types, comparing both linear and nonlinear elasticity cases.

2 Theoretical Considerations

2.1 Problem Formulation

Consider a random heterogeneous material $\mathbf{B} = \{B(\omega);\ \omega \in \Omega\}$, where each point ω corresponds to a sample space Ω and $B(\omega)$ is a specific realization of some spatial (2-D or 3-D) random process. Here we distinguish two phases: matrix $B_1(\omega)$ and inclusion $B_2(\omega)$, although the results presented in the paper can readily be extended to multiphase materials. Generally speaking,

the random medium is described by a distribution of phases, such that $B_1(\omega) \cup B_2(\omega) = B(\omega)$ and $B_1(\omega) \cap B_2(\omega) = 0$ [24], which can be set up on the basis of point fields. While in the periodic homogenization one is usually concerned with phase distribution within the periodic window directly taken as the RVE (Figure 1a), the homogenization in random media can be carried out only if a spatial homogeneity assumption is imposed. This implies invariance of probability distributions under arbitrary translations. Additionally, we require the random medium to be ergodic:

$$\langle F \rangle = \lim_{V_0 \to \infty} \frac{1}{V_0} \int_{V_0} F dV, \tag{2}$$

where $\langle \bullet \rangle$ denotes ensemble average and V_0 is material volume in reference state.

2.2 Mesoscale Bounds on Effective Strain Energy Function

The major difference between linear and nonlinear elasticity in terms of a bounding problem is that the hierarchy of bounds on effective properties in nonlinear elasticity, except for some special cases [7], cannot be obtained in the tensor form and the full strain energy function has to be considered.

The equation of state of the material in nonlinear elasticity can be written in the following form

$$P_{ij} = \frac{\partial \psi}{\partial F_{ij}}, \tag{3}$$

where ψ is a strain energy function per unit volume of an undeformed body, P_{ij} is the first Piola-Kirchhoff stress tensor and F_{ij} is the deformation gradient tensor. It must be noted that the constitutive relation (3) is given in a material description. The reason for it is that the average strain theorem in finite elasticity can be formulated for the deformation gradient tensor only [25, 26]. Moreover, most of the strain energy functions commonly employed in the literature are defined in a reference configuration.

The principal idea behind the derivation of mesoscale bounds is the introduction of two types of boundary conditions – *restricted* (the boundary condition specified on the boundary of a window of size $\delta' = \frac{\delta}{n}$, where n is nonnegative and nonzero) and *unrestricted*

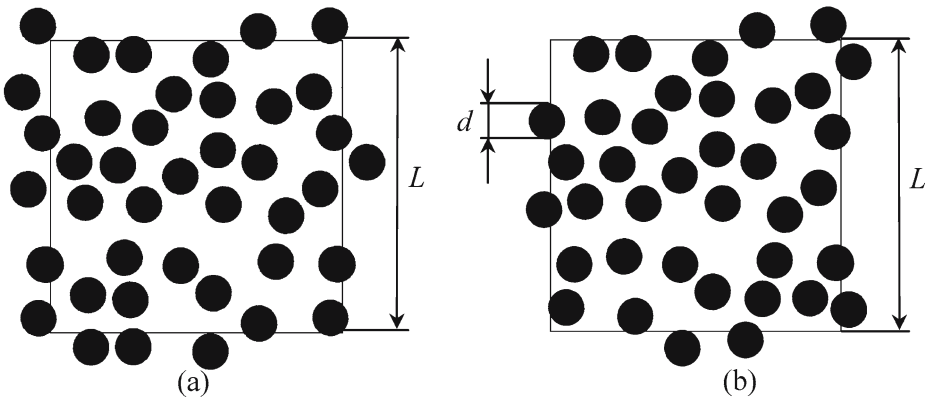

Figure 1 (a) A disordered microstructure of a periodic composite with a periodic window of size L; (b) one realization of a random composite $B_\delta(\omega)$ of size L.

(the boundary condition specified on the boundary of window δ), and subsequent application of variational principles of minimum potential and complementary energies in finite elasticity [27], as well as the Hill (or Hill-Mandel) condition [25]

$$\overline{P_{ij}F_{ij}} - \overline{P}_{ij}\overline{F}_{ij} = \frac{1}{V_0}\int_{S_0}\left(t_i - \overline{P}_{ij}n_j\right)\left(u_i - \left(\overline{F}_{ij} - \delta_{ij}\right)X_j\right)dV = 0. \tag{4}$$

Here the superposed bar denotes the volume average, n_j is an outward normal vector to the boundary surface in the reference configuration, X_j denotes the coordinates of a particle inside the body in the reference configuration, δ_{ij} is the Kronecker delta, and indices i, j range over the values 1, 2, 3. Condition (4) insures independence of volume-averaged properties of the composite from the applied boundary conditions and can be satisfied in three different cases:

(1) kinematic uniform boundary condition (KUBC):

$$u_i^0 = \left(F_{ij}^0 - \delta_{ij}\right)X_j,\ \forall X_j \in S_0\,; \tag{5}$$

(2) static uniform boundary condition (SUBC):

$$t_i^o = P_{ij}^0 n_j,\ \forall X_j \in S_0\,; \tag{6}$$

(3) uniform orthogonal-mixed boundary condition (MIXED):

$$\left(t_i - P_{ij}^0 n_j\right)\left(u_i - \left(F_{ij}^0 - \delta_{ij}\right)X_j\right) = 0,\ \forall X_j \in S_0, \tag{7}$$

where the averaging theorems [25, 26] have been used.

Following the procedure outlined in [23], one can derive two hierarchies of mesoscale bounds on the effective strain energy function: the upper bound obtained under KUBC Equation (5)

$$\left\langle\Psi\left(\mathbf{F}^0\right)\right\rangle_\Delta \le \left\langle\Psi\left(\mathbf{F}^0\right)\right\rangle_\delta \le \left\langle\Psi\left(\mathbf{F}^0\right)\right\rangle_{\delta'} \le \left\langle\Psi\left(\mathbf{F}^0\right)\right\rangle_1, \text{for } 1 < \delta' < \delta < \Delta, \tag{8}$$

where

$$\Psi\left(\omega, \mathbf{F}^0\right) = \int_{V_0}\Psi(\omega, X, F)dV$$

and Δ and 1 denote the RVE size and inhomogeneity size, respectively, and the lower bound obtained under SUBC (6)

$$\left\langle\Psi^*\left(\mathbf{P}^0\right)\right\rangle_\Delta \le \left\langle\Psi^*\left(\mathbf{P}^0\right)\right\rangle_\delta \le \left\langle\Psi^*\left(\mathbf{P}^0\right)\right\rangle_{\delta'} \le \left\langle\Psi^*\left(\mathbf{P}^0\right)\right\rangle_1, \text{for } 1 < \delta' < \delta < \Delta, \tag{9}$$

where

$$\Psi^*\left(\omega, \mathbf{P}^0\right) = \int_{V_0}\left\{\frac{\partial\Psi}{\partial U_{ij}}U_{ij} - \Psi\right\}dV$$

and U_{ij} is an admissible deformation gradient field.

At the macroscale $\Psi(\omega, \mathbf{F}_0) = \Psi(\omega, \mathbf{P}_0)$ and $\Psi^*(\omega, \mathbf{P}_0) = \Psi^*(\omega, \mathbf{F}_0)$ so that, we recover the regular Legendre transformation

$$\Psi = \mathbf{P} : \mathbf{F} - \Psi^*. \tag{10}$$

This property will allow us to estimate the lower bound on the strain energy function as $\delta \to \infty$ (see "Numerical Experiments Section 3").

It is important to mention, that, contrary to the linear theory, the hierarchy (8) is valid only if certain restrictions are imposed on the strain-energy function, namely, if

$$\int_{V_0} \frac{\partial^2 \psi}{\partial u_{i,k} \partial u_{p,q}} d_{i,k} d_{p,q} dV > 0 \tag{11}$$

for all nonzero d_i such that $d_i = 0$ on the part of the bounding surface S_0 where displacements are prescribed S_U. On the other hand, the hierarchy (9) is valid if

$$\int_{V_0} \frac{\partial^2 \psi}{\partial u_{i,k} \partial u_{p,q}} d_{ik} d_{pq} dV > 0 \tag{12}$$

for all nonzero d_{ik} satisfying $\frac{\partial}{\partial x_k}\left(\frac{\partial^2 \psi}{\partial u_{i,k} \partial u_{p,q}} d_{pq}\right) = 0$ in V_0 and $\frac{\partial^2 \psi}{\partial u_{i,k} \partial u_{p,q}} d_{pq} n_k = 0$ on the part of S_0 where the traction is prescribed S_T.

In the small deformation theory the effective strain energy function $\Psi_{eff} = \frac{1}{2}\boldsymbol{\varepsilon}$: $\mathrm{C}_{eff} : \boldsymbol{\varepsilon}$ is equal to the complementary energy function $\Psi^*_{eff} = \frac{1}{2}\boldsymbol{\sigma}$: $\mathrm{S}_{eff} : \boldsymbol{\sigma}$ and hierarchies (8) and (9) can be combined to give [17]:

$$\begin{aligned} \left\langle \mathbf{S}_1^{\sigma} \right\rangle^{-1} \le \cdots \le \left\langle \mathbf{S}_{\delta'}^{\sigma} \right\rangle^{-1} \le \left\langle \mathbf{S}_{\delta}^{\sigma} \right\rangle^{-1} \le \cdots \le \mathbf{S}_{eff}^{-1} = \mathbf{C}_{eff} \le \cdots \le \left\langle \mathbf{C}_{\delta}^{\varepsilon} \right\rangle \le \left\langle \mathbf{C}_{\delta'}^{\varepsilon} \right\rangle \le \cdots \\ \le \left\langle \mathbf{C}_1^{\varepsilon} \right\rangle. \end{aligned} \tag{13}$$

Here the superscripts $\boldsymbol{\varepsilon}$ and σ define properties obtained under boundary conditions (5) and (6), which in linear elasticity reduce to $u_i^0 = \varepsilon_{ij}^0 x_j$ and $t_i^0 = \sigma_{ij}^0 n_j$, correspondingly. Here $\boldsymbol{\varepsilon}$ is the strain tensor, $\boldsymbol{\sigma}$ is the Cauchy stress tensor, $\mathbf{C}$ is the stiffness tensor and $\mathbf{S}$ is the compliance tensor.

2.3 Classical Bounds

Early theoretical studies on bounding of effective properties in linear elasticity were carried out by Voigt and Reuss, who proposed approximations for the effective material properties based on simplifying assumptions, respectively, of a uniform strain or uniform stress fields inside the composite. A generalization of the above mentioned bounds in the context of finite elasticity was first carried out by Ogden [28] for a convex strain energy function. A more general assumption of polyconvexity of ψ was later considered by Ponte Castañeda [29].It follows from the minimum potential energy theorem that under kinematic uniform boundary conditions

$$\int_{V_0} \psi\left(u_{i,k}, X_j\right) dV \le \int_{V_0} \psi\left(\overline{u}_{i,k}\right) dV \tag{14}$$

or

$$\langle \Psi \rangle_{\Delta} \le \overline{\Psi}, \tag{15}$$

which provides a *strict* upper bound on material properties. Indeed, as δ approaches zero, the displacement gradient field within the composite becomes more and more uniform

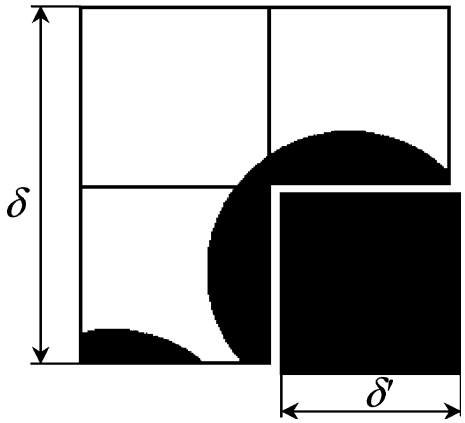

Figure 2 Partitioning of a window of scale δ into four squares of scale $\delta' < 1$.

(Figure 2), which finally results in the strain energy function tending to a simple weighted average of the energy functions of both phases:

$$\left\langle \Psi\left(\mathbf{F}^0\right)\right\rangle_{\delta\to 0} = V_1\psi_1\left(\mathbf{F}^0\right) + V_2\psi_2\left(\mathbf{F}^0\right). \tag{16}$$

The Reuss bound can be obtained in the same fashion from the complementary energy theorem:

$$\left\langle \Psi^*\right\rangle_{\Delta} \le \overline{\Psi^*}. \tag{17}$$

In practice, the bound (17) is of little use since the complementary energy function in nonlinear elasticity is generally unknown. We shall therefore investigate the strict lower bound in a different way. Consider the complementary energy functional in the form

$$Q\{U_{ij}\} = \int_{V_0}\left\{\frac{\partial\psi}{\partial U_{ij}}U_{ij} - \psi\right\}dV - \int_{S_U}\frac{\partial\psi}{\partial U_{ij}}n_j x_i^0 dS, \tag{18}$$

where x_i^0 denotes the coordinates of a particle inside the body in the current configuration. Under the kinematic uniform boundary condition $S_U = S_0$ and upon application of the Green–Gauss theorem, the functional (18) reduces to

$$Q\{U_{ij}\} = -\int_{V_0}\psi dV. \tag{19}$$

At the same time, for an admissible stress field in the composite we have either

$$Q\{P_{ij}\} \le Q\{\overline{P}_{ij}\} \tag{20}$$

or

$$\langle\Psi\rangle_{\Delta} \ge \overline{\Psi}\left(\overline{\mathbf{P}}\right), \tag{21}$$

which provides a strict lower bound on the effective strain energy function.

Note, that the Voigt / Reuss bounds don't give any information on the size of the RVE and, while rigorous, provide a very bad estimate of the effective material properties. As is well known, the Hashin–Shtrikman bounds [29, 30] also provide bad estimates as the phases' mismatch in the microstructure grows. By contrast, the bounds investigated in the current study are progressively tight with the mesoscale growing.

3 Numerical Experiments

3.1 Material Model

To illustrate and investigate the convergence of mesoscale bounds to the RVE response, we consider a material made of an elastomeric matrix with embedded, randomly distributed nonlinear elastic inclusions. Such a composite is often employed in industry to enhance mechanical properties of polymeric materials [31], to improve their toughness [32, 33], impact strength [34], etc. It also models some biological tissues [35].

Here we study a two-dimensional nonlinear composite with the microstructure modeled through a planar homogeneous Poisson point process with a probability mass function defined as

$$P\{N(A) = k\} = e^{-\lambda(A)} \frac{\lambda(A)^k}{k!}, A \subset \mathbf{R}^2, \tag{22}$$

where $N(A)$ is a number of successful trials and $\lambda(A)$ is a parameter defined as

$$\lambda(A) = f \frac{\text{Area}(B(\omega))}{\text{Area}(A)}, \tag{23}$$

where f is a prescribed volume fraction of inclusions. Poisson points are generated in such a way that no two points may be closer than a certain distance $D = 1.1d$, where d is the diameter of the inclusions. Imposing this non-overlap condition allows us to avoid numerical difficulties associated with narrow necks between inclusions, which can be crucial in simulations involving finite deformations.

For numerical simulations we consider a compressible isotropic hyperelastic material of Ogden type [36] with the strain energy function given by

$$\begin{aligned} \psi &= \sum_{i=1}^{N} \frac{2\mu_i}{\alpha_i^2} \left(\widetilde{\lambda}_1^{\alpha_i} + \widetilde{\lambda}_2^{\alpha_i} + \widetilde{\lambda}_3^{\alpha_i} - 3 \right) + \sum_{i=1}^{N} \frac{1}{D_i} (J-1)^{2i}, \\ \widetilde{\lambda}_a &= J^{-\frac{1}{3}} \lambda_a, \end{aligned} \tag{24}$$

where λ_a are principal values of the deformation gradient, J is the Jacobian and N, μ_i, α_i, and D_i are material parameters. Classical (initial) shear μ_0 and bulk modulus κ_0 in the reference configuration for the Ogden form are related to the material parameters by the expressions

$$\mu_0 = \sum_{i=1}^{N} \mu_i, \tag{25}$$

$$\kappa_0 = \frac{2}{D_1}. \tag{26}$$

When dealing with a nonlinear composite it is not clear how to define mismatch between the phases, especially when they are described by two different forms of the strain energy

function. While most engineering materials for which linear elasticity theory is applicable are compressible, the hyperelastic response is characterized by near incompressibility. For a typical elastomer the initial bulk modulus exceeds the shear modulus by 1,000 to 10,000 times and, therefore, a mismatch (or contrast) between two phases α in the hyperelastic composite would be more logically defined in terms of the initial shear modulus rather than in terms of the bulk modulus or material parameters in general.

The physical properties of the materials used in the illustrative examples of this paper are listed in Table 1. Material 1 defines a typical rubber [36] and materials 2 and 3 are of neo-Hookean type [37], which, as can be seen from the table, can be obtained as a special case of a general Ogden strain energy potential (24). The neo-Hookean type strain energy function is the simplest form of ψ and is a generalization of a linear stress–strain relation in finite elasticity. It provides good agreements with experiments within a small strain domain and therefore is preferable to be employed when deformations are relatively small.

It is worth mentioning that the strain energy potential (24) with parameters defined in Table 1 satisfies inequalities (11) and (12) and therefore bounds (8) and (9) hold over all admissible deformations.

To illustrate and compare the convergence of bounds (8) and (9), we investigate four nonlinear elastic composites of the following types:

No. 1: neo-Hookean inclusions in Ogden matrix with $\frac{\mu_0^{(i)}}{\mu_0^{(m)}} = 10$,

No. 2: Ogden inclusions in neo-Hookean matrix with $\frac{\mu_0^{(i)}}{\mu_0^{(m)}} = 0.1$,

No. 3: neo-Hookean inclusions in neo-Hookean matrix with $\frac{\mu_0^{(i)}}{\mu_0^{(m)}} = 10$,

No. 4: neo-Hookean inclusions in neo-Hookean matrix with $\frac{\mu_0^{(i)}}{\mu_0^{(m)}} = 0.1$, as well as two linear elastic composites:

No. 5: $\frac{\mu^{(i)}}{\mu^{(m)}} = 10$, $\frac{\kappa^{(i)}}{\kappa^{(m)}} = 10$,

No. 6: $\frac{\mu^{(i)}}{\mu^{(m)}} = 0.1$, $\frac{\kappa^{(i)}}{\kappa^{(m)}} = 0.1$,

where μ is the shear modulus and κ is the bulk modulus. The volume fraction of inclusions is chosen to be 0.35; perfect bounding between matrix and inclusions is assumed.

3.2 Discretization

The finite element analysis is carried out using the software ABAQUS 6.5. The discretization is performed with a non-uniform mesh (Figure 3), generated automatically with the use of the ABAQUS scripting interface. Such a mesh shows a significantly better convergence to the true solution with a smaller number of degrees of freedom (DOF)

Table 1 Material properties used in the computational examples

Material	Material parameters	Initial shear modulus (N/m^2)
Ogden type	$N = 3$, $\mu_1 = 4.095 \times 10^5$ N/m^2, $\alpha_1 = 1.3$ $\mu_2 = 0.03 \times 10^5$ N/m^2, $\alpha_2 = 5.0$ $\mu_3 = 0.1 \times 10^5$ N/m^2, $\alpha_3 = -2.0$ $D_1 = 4.733 \times 10^{-8}$ N/m^2, $D_2 = 0$, $D_3 = 0$	$\mu_0 = 4.225 \times 10^5$
Neo-Hookean type	$N = 1$, $\mu_1 = 42.25 \times 10^5$ N/m^2, $\alpha_1 = 2.0$ $D_1 = 4.733 \times 10^{-8}$ N/m^2	$\mu_0 = 42.25 \times 10^5$
Neo-Hookean type	$N = 1$, $\mu_1 = 4.225 \times 10^5$ N/m^2, $\alpha_1 = 2.0$ $D_1 = 4.733 \times 10^{-8}$ N/m^2	$\mu_0 = 4.225 \times 10^5$

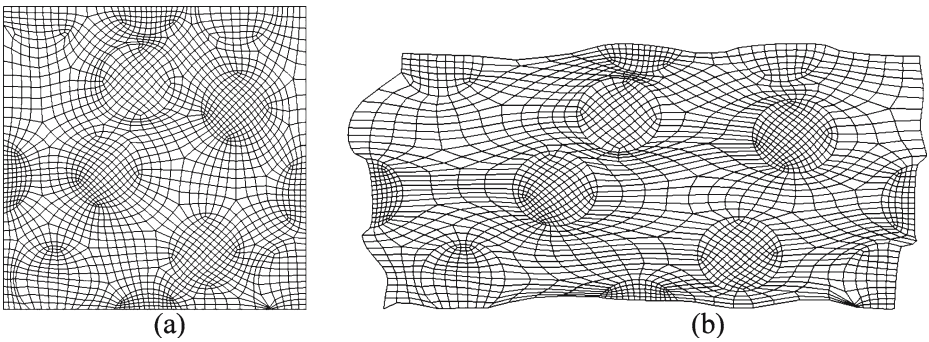

Figure 3 The finite element mesh of a composite in (a) undeformed and (b) deformed (traction boundary conditions) configurations.

compared to the square shaped uniform mesh. Over a series of repetitive refinements, an average element size of 0.75 for $d = 10$ (approximately 450 DOF for $\delta = 1$ and 70,500 DOF for $\delta = 16$) was found to produce mesh independent results. Four-node bilinear elements with full integration are used in the analysis.

3.3 Ensemble Averaging

Before proceeding with numerical experiments, the number of microstructural assembles for each window size δ must be investigated. As the window size is increasing, the probability of occurrence of extremely high or small values of the stored strain energy becomes smaller. As a result, the standard deviation σ decreases approaching zero as $\delta \to \infty$ (for the discussion of the dependence of the standard deviation on δ see "Statistical Approach to the RVE Size Estimation Section 3.4.2"). Thus, the larger is the window size, the lower is the number of numerical experiments required to obtain statistically representative results. The following numbers of realizations of a random composite were generated: 512 for $\delta = 1$; 384 for $\delta = 2$; 160 for $\delta = 4$; 40 for $\delta = 8$; 10 for $\delta = 16$.

It is interesting to determine the probability density function that describes the energy density distribution of the composite at different scales. Such an analysis was carried out for the nonlinear composite No. 1. It was found that the distribution function does depend on the scale, however averaging over all scales showed that, for both displacement and traction boundary conditions, the Beta and Chi distributions give the best fit among all the classical distributions with a 0.8% difference in the Kolmogorov–Smirnov test statistic. The plot of the corresponding Beta functions for each scale is given in Figure 4. With the increasing window size, the probability density function flows away from end points converging to the Dirac delta as $\delta \to \infty$. Moreover, depending on the boundary conditions, the mean value shifts to the right or to the left. The negative sign of the strain energy in Figure 4b is a result of the way we calculate the energy density under traction boundary condition (10), and this is described in more detail in the next section.

3.4 Numerical Results

3.4.1 Bounds on Effective Properties

If the microstructure statistics admits isotropy, then, upon ensemble averaging (which involves integration over all the realizations of the random microstructure), the

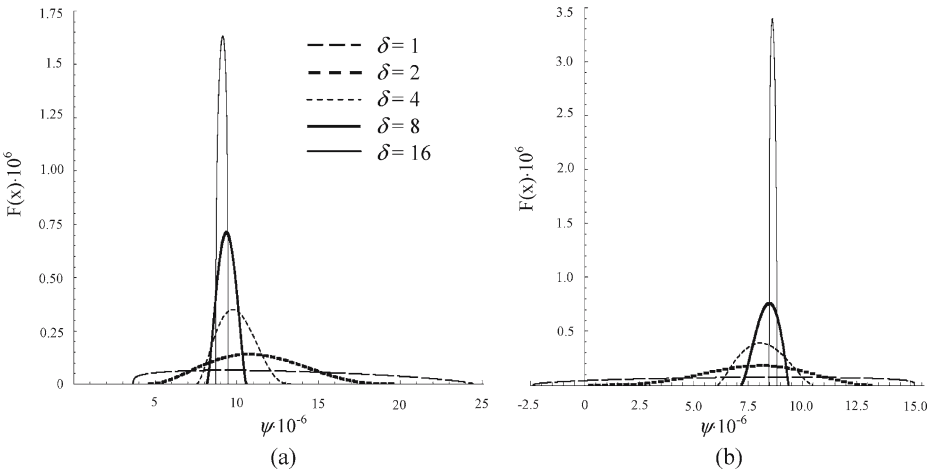

Figure 4 Probability densities for the stored strain energy density of the nonlinear composite No. 1 under (a) uniform displacement and (b) uniform traction boundary conditions.

microstructure response is isotropic – no material direction has any preference. This reasoning is implicitly involved in the development of constitutive laws of materials in deterministic continuum mechanics. If sufficiently many realizations of a composite are taken to remove the directional dependence, then isotropy of the ensemble-averaged response is also very well supported by numerical simulations. For example, in linear elasticity computational results show that $\langle \mathbf{C}_\delta \rangle$ is an isotropic forth-rank tensor [15], whereas in nonlinear elasticity the ensemble average stress under KUBC has zero shear components, which can be expected only for an isotropic response. Analogous results are obtained under static uniform boundary conditions for the ensemble averaged deformation gradient tensor.

Hence, in the following, we take $\langle \psi_\delta \rangle$ to be an isotropic scalar valued function of $\mathbf{F}$ and treat the ensemble averaged material response of the nonlinear composite as generally isotropic. Consequently, the stored energy function $\langle \psi_\delta \rangle$ may be regarded as a symmetric function of the three extension ratios λ_a.

For a good description of hyperelastic materials, more than one type of test is required. If only one test is performed, the non-uniqueness of material parameters fitted to the experimental data may occur [38]. This is particularly important when the material is defined by a complex strain-energy function, such as the one given by (24).

Generally, any deformation mode can be investigated. However, from the experimental standpoint, the most common deformation modes are considered to be sufficient to determine material coefficients [36]. Here we assume plane stress deformations and consider three different deformation modes: uniaxial tension, equibiaxial tension and pure shear, along with three types of boundary conditions summarized in Table 2.

It is very difficult to obtain pure shear response in the nonlinear composite under SUBC specified in the reference configuration (see (6)) unless deformations of the material are known *a priori*. Moreover, since the surface traction applied on the boundary of the sample is a dead load, numerical difficulties associated with excessive finite element distortions in shear and boundary contact make determination of the stress–strain curve almost impossible. Note, that the dead load assumption allows us to use variational principles in the derivation of mesoscale bounds without placing any limitation on the choice of statically admissible stress.

Table 2 Boundary conditions used in the computational examples

Deformation modes	Uniaxial tension	Equibiaxial tension	Pure shear
Static uniform b.c. (SUBC)	$P^0_{11} = P,$ $P^0_{22} = P^0_{12} = P^0_{21} = 0$	$P^0_{11} = P^0_{22} = P$ $P^0_{12} = P^0_{21} = 0$	–
Kinematic uniform b.c. (KUBC)	$F^0_{11} = \langle\overline{\lambda_1}\rangle^{\mathbf{P}}, F^0_{22} = \langle\overline{\lambda_2}\rangle^{\mathbf{P}},$ $F^0_{12} = F^0_{21} = 0$	$F^0_{11} = F^0_{22} = \lambda,$ $F^0_{12} = F^0_{21} = 0$	$F^0_{11} = \lambda, F^0_{22} = \frac{1}{\lambda},$ $F^0_{12} = F^0_{21} = 0$
Orthogonal-mixed b.c. (MIXED)	$F^0_{11} = \langle\overline{\lambda_1}\rangle^{\mathbf{P}}, F^0_{22} = \langle\overline{\lambda_2}\rangle^{\mathbf{P}},$ $P^0_{12} = P^0_{21} = 0$	$F^0_{11} = F^0_{22} = \lambda,$ $P^0_{12} = P^0_{21} = 0$	$F^0_{11} = \lambda, F^0_{22} = \frac{1}{\lambda},$ $P^0_{12} = P^0_{21} = 0$

Orthogonal-mixed boundary conditions specified in Table 2 reproduce a common experimental setup, when displacements are applied without friction on all sides of the specimen (Figure 5). These boundary conditions are important from a practical viewpoint as they allow one to compare numerical simulations with experimental results.

Figures 6 and 7 present two examples of a nonlinear composite response under uniaxial loading. From the stress–strain curves we observe that the effective response for both composites is bounded from above by a response under displacement boundary conditions and from below by a response under traction boundary conditions. Orthogonal-mixed boundary conditions give an intermediate result for $\delta > 2$ and tend to overestimate the effective response for smaller window sizes. It is interesting to note that, while in the first composite (where matrix is represented by a soft Ogden type material) the curves change their shape gradually from the neo-Hookean to Ogden type response, in the second composite the curves are more shifted toward the hard phase. Analogous results were obtained for all considered deformation modes, which we do not present here for the sake of brevity.

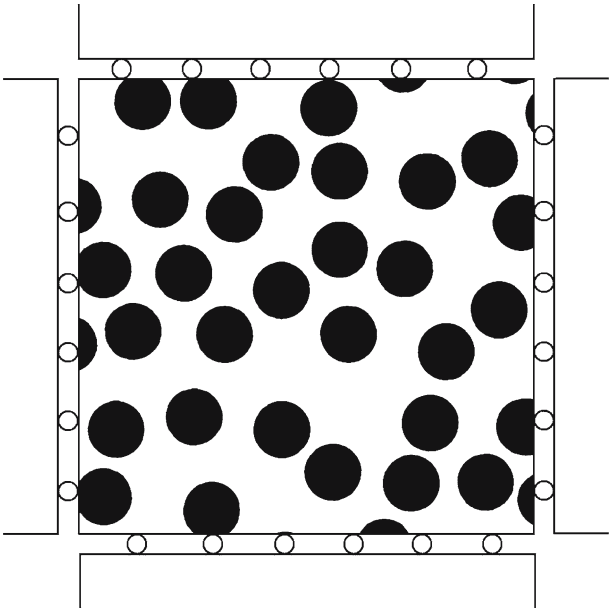

Figure 5 Loading under orthogonal-mixed boundary condition.

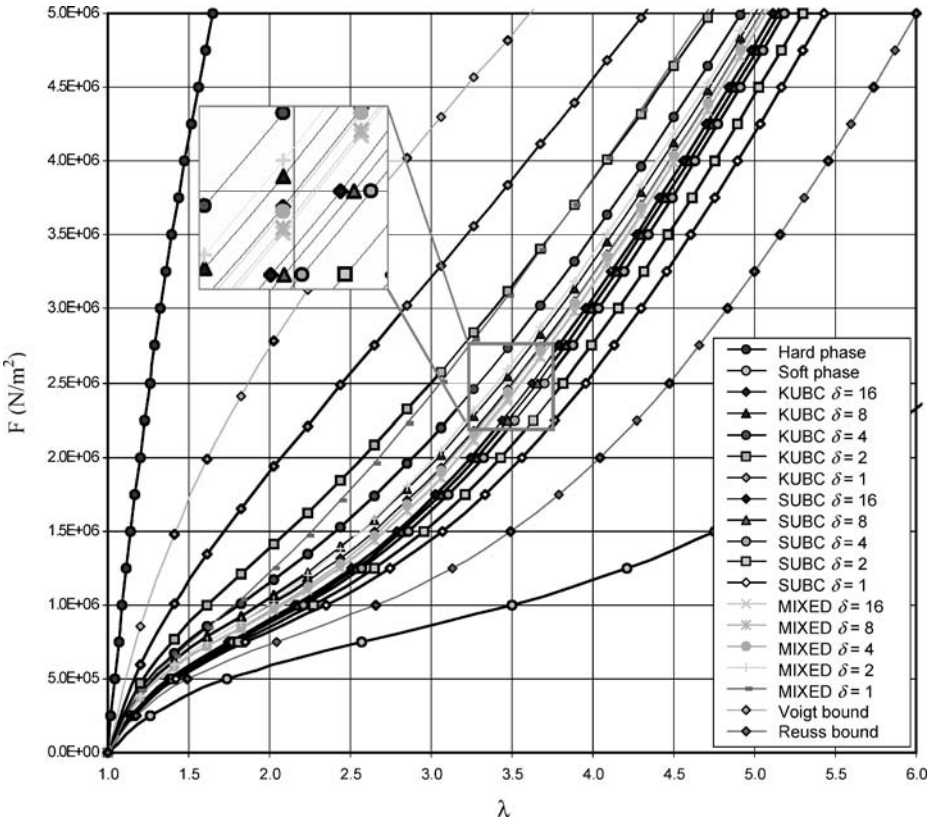

Figure 6 Stress – strain curves of a random composite No. 1 under uniaxial loading.

The material coefficients were computed for each stress–strain data set using standard fitting procedure and the Ogden model with $N = 1$, $N = 2$, $N = 3$ [38]. It was found that for composite No. 1 the strain-energy function with three terms provides the best fit up to $\delta = 2$ under KUBC, whereas the one term strain energy function and the neo-Hookean model give better results for $\delta = 1$ under KUBC and for the Voigt bound, respectively. An opposite situation is encountered for the composite No. 2, where the three terms Ogden function is slowly changing to a two terms function at $\delta = 2$ under SUBC, and then to a neo-Hookean model at $\delta = 16$ under KUBC. Unfortunately, here we cannot mathematically describe the transition of each material parameter from the lower to the upper bound. The reason for it is that even a slight change in material response produces a completely different set of fitted material parameters, and therefore there is no continuous transition for individual coefficient from one scale to another. The only material parameter, for which the scale dependence can be defined mathematically, is the initial shear modulus (Figure 8). Indeed, it was found that

$$\mu_0^t = A \exp[m\delta] - B \exp[-n\delta], \tag{27}$$

$$\mu_0^d = C \exp[-k\delta] + D \exp[-p\delta], \tag{28}$$

where A, m, B, n, C, k, D and p are parameters evaluated through a nonlinear least-square fitting procedure (Table 3).

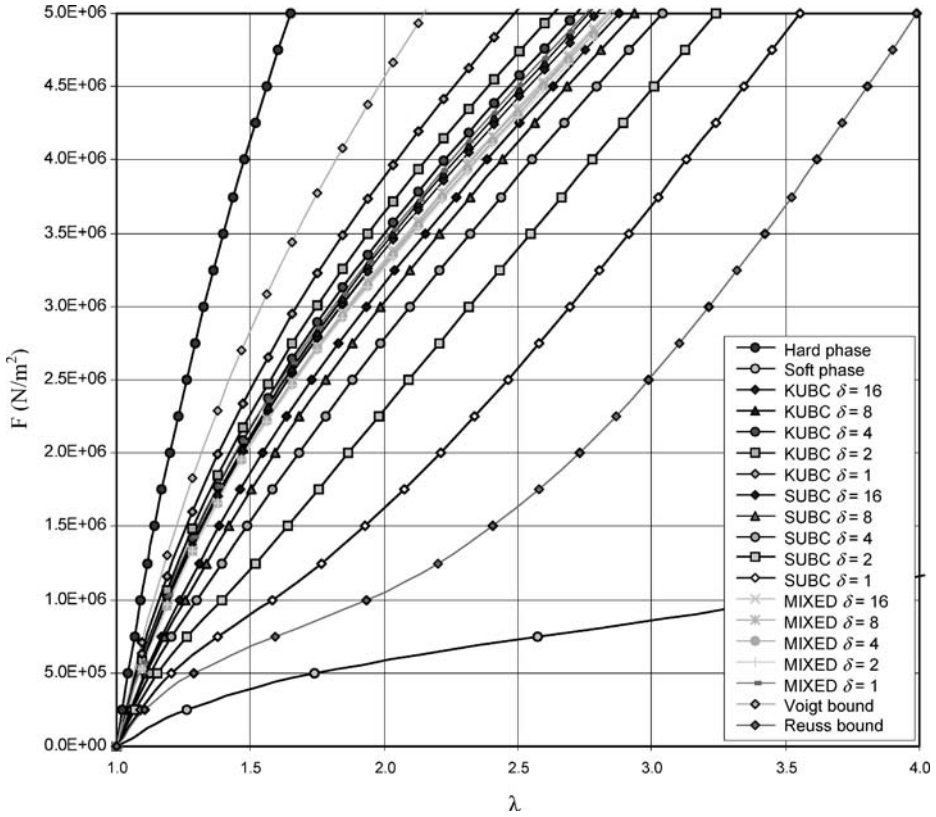

Figure 7 Stress – strain curves of a random composite No. 2 under uniaxial loading.

Under KUBC for the composite No. 1 the difference of approximately 30% occurred between the initial shear modulus of samples 2 and 16 times bigger than the heterogeneity size, whereas under SUBC the difference is only 2%. An opposite result is encountered for the composite with soft inclusions (No. 2): 9% difference under KUBC and 33% under SUBC. It is interesting to note that the studies of a linear microstructure with random distribution of pores, modeled as soft inclusions [10], revealed the difference of 2.6% for effective shear response under KUBC. Our study shows, that results obtained under KUBC only might lead to a wrong estimation of the RVE. Thus, for a reliable estimate one has to consider the convergence of both bounds.

The curve fitting for neo-Hookean type composites showed that all the ensemble-averaged responses are best represented by the neo-Hookean form. The slight deviations from the neo-Hookean model are small compared to the other forms. Analogous observations for the effective material response were made in [19].

A strain-energy density is a function of three principal stretches and therefore it has different values for different boundary conditions. To demonstrate the convergent trends of bounds (8) and (9) we will consider each deformation mode given in Table 2 and proceed with the following steps:

1) Compute response under SUBC and obtain $\langle \Psi^*(\mathbf{P}^0) \rangle_\delta$;
2) Apply KUBC through $\lambda_i^0 = \langle \overline{\lambda_i} \rangle^{\mathbf{P}}_{\delta=\delta_{\max}}$ and obtain $\langle \Psi(\mathbf{F}^0) \rangle_\delta$;

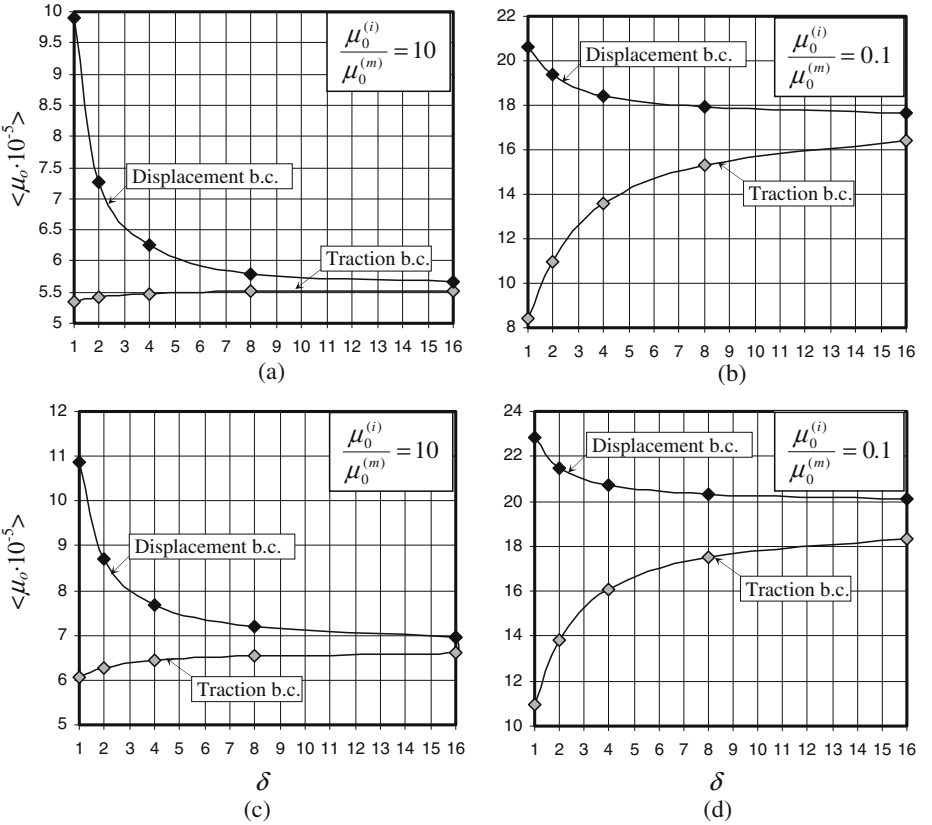

Figure 8 Bounds on the initial shear modulus for different composites: (a) No. 1, (b) No. 2, (c) No. 3, (d) No. 4.

3) Compute lower bound on the strain energy function using the following relation:

$$\left\langle \Psi\left(\mathbf{P}^0\right)\right\rangle_\delta = \mathbf{P}_{\delta=\delta_{\max}} : \mathbf{F}_{\delta=\delta_{\max}} - \left\langle \Psi^*\left(\mathbf{P}^0\right)\right\rangle_\delta. \tag{29}$$

With increasing δ, the gap between $\left\langle \Psi\left(\mathbf{F}^0\right)\right\rangle_\delta$ and $\left\langle \Psi\left(\mathbf{P}^0\right)\right\rangle_\delta$ becomes smaller, and this can then be used to estimate the size of the RVE with a desired accuracy. In our numerical analysis we choose $\delta_{\max} = 16$, given the limitation of our computer (11 GB of random access memory).

The results for two nonlinear composites are shown in Figure 9. The values are normalized with respect to the Voigt bound. The numerical simulations support theoretically derived results (8) and (9): the natural boundary condition provides the upper bound, while the essential boundary condition provides the lower bound. The comparison shows that for

Table 3 Parameters in equations (26) and (28) for different composite models

Composite	$A \times 10^{-5}$	m	$B \times 10^{-5}$	n	$C \times 10^{-5}$	k	$D \times 10^{-5}$	p
1	5.5	0.0004	0.3	0.766	6.2	0.0076	11.9	1.172
2	14.6	0.0065	10.3	0.472	18.7	0.0017	4.7	0.656
3	6.5	0.0010	0.8	0.635	7.6	0.0058	8.9	1.001
4	16.8	0.0054	10.7	0.587	20.6	0.0017	5.2	0.858

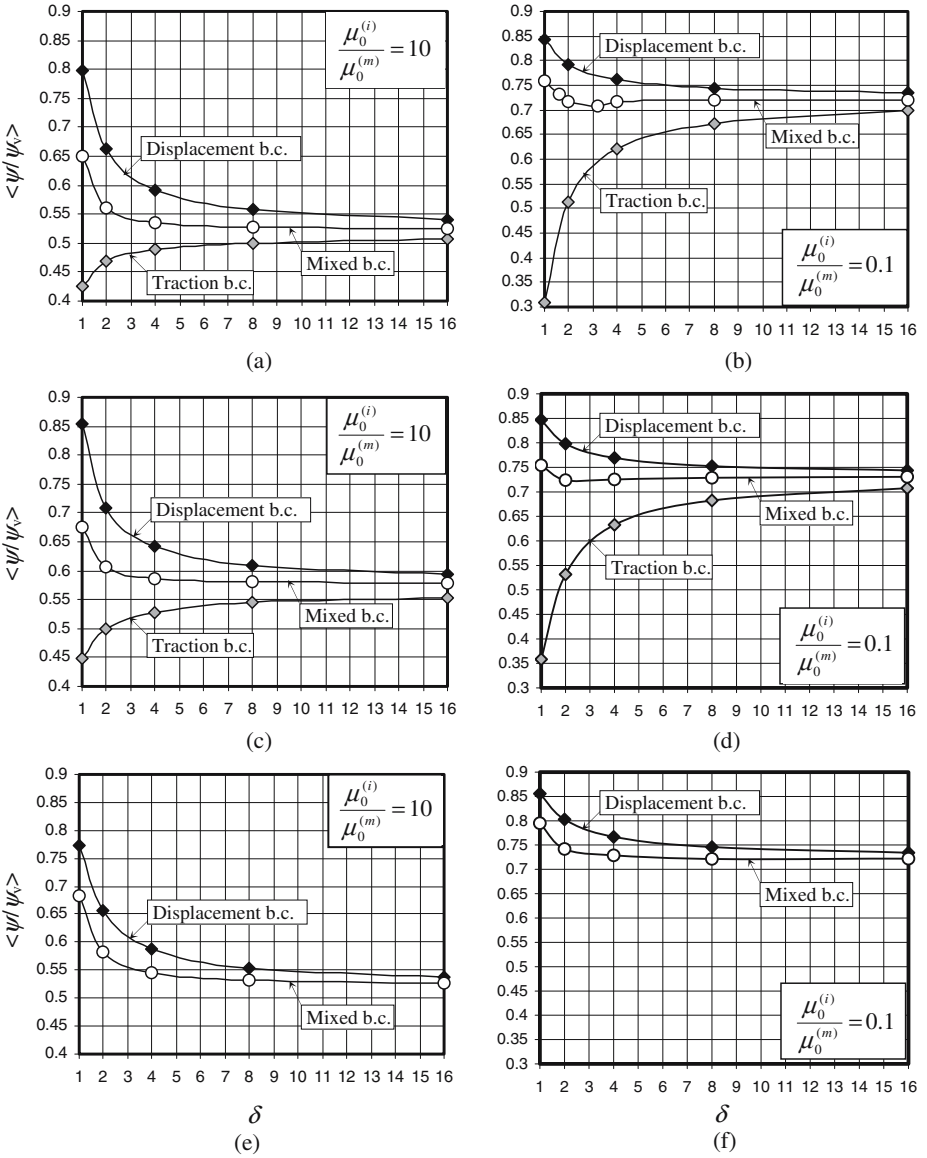

Figure 9 Energy bounds for the nonlinear random composite of Ogden – neo-Hookean type (No. 1 and No. 2) under (a), (b) uniaxial tension, (c), (d) biaxial tension, (e), (f) pure shear.

all deformation modes the hierarchical trends are similar. However, when the matrix is soft, the lower bound converges faster, whereas for a composite with the hard matrix the lower bound approaches the effective value slower than the upper one. An analogous conclusion can be made for all the studied composites (see Figures 9, 10 and 11).

As expected from the stress–strain response, the mixed boundary condition yields an intermediate result, which asymptotes rapidly. This can be used to estimate the effective response without an initial determination of the RVE size.

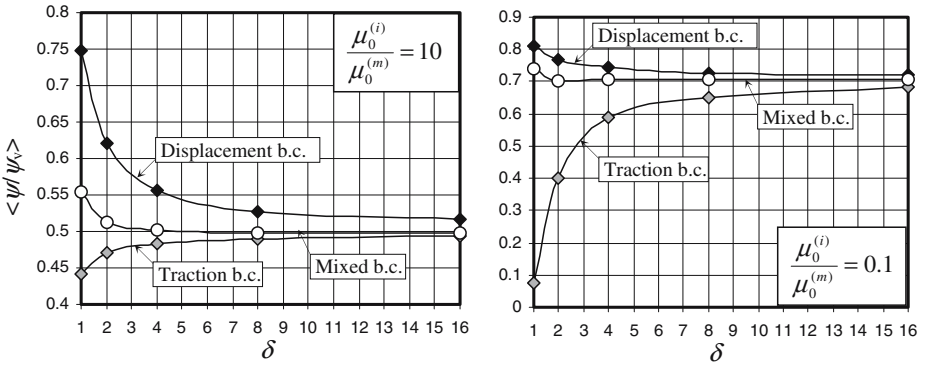

Figure 10 Energy bounds for the nonlinear random composite of neo-Hookean – neo-Hookean type (No. 3 and No. 4) under uniaxial tension.

When $\delta \to 0$, samples can be considered to be homogeneous with the material corresponding to either matrix or inclusions and mixed boundary conditions become identical to displacement controlled boundary conditions. This is the reason why the response under the mixed boundary condition also converges from above. It can be noticed that for composites with $\frac{\mu_0^{(i)}}{\mu_0^{(m)}} = 0.1$, the response under the mixed boundary condition does not decay monoton-

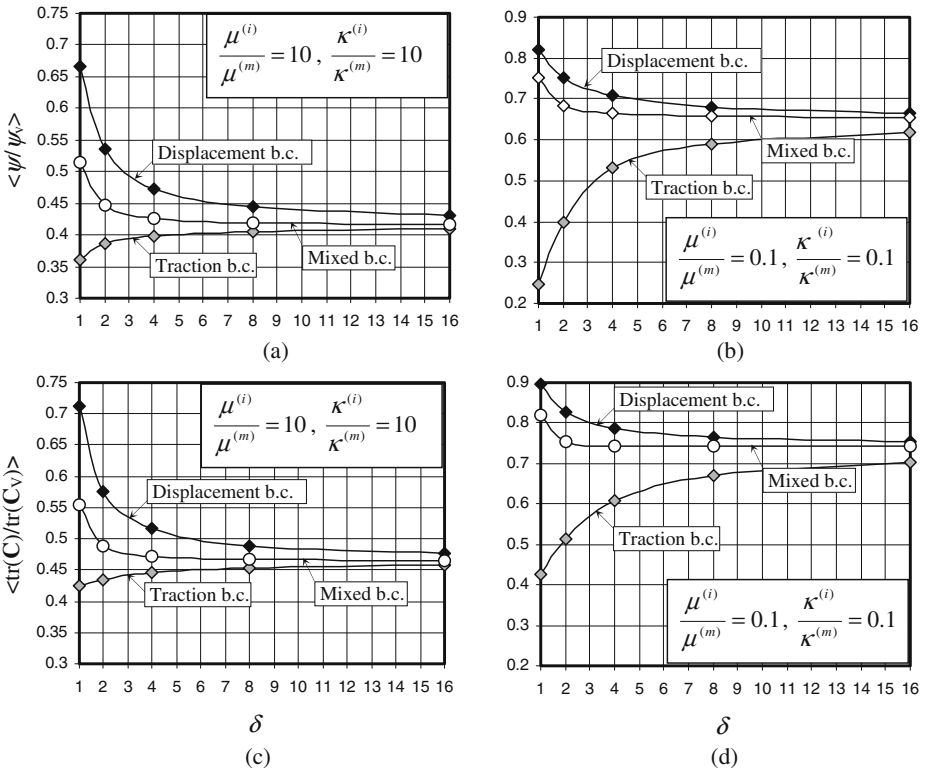

Figure 11 Bounds on the strain energy (a, b) and material properties (c, d) of the linear elastic composite (No. 5 and No. 6) under uniaxial tension.

ically: it shifts in the range of $1 < \delta < 4$ for all nonlinear materials under uniaxial and biaxial tension.

In Figure 11 we compare mesoscale bounds on the strain energy function with the bounds on the effective stiffness tensor in linear elasticity. These bounds represent different quantities and are computed under different boundary conditions. To estimate the convergence of the *strain energy* we first compute the response under SUBC and then apply the ensemble-averaged strain in KUBC using only *one* set of boundary conditions defined above. In order to estimate apparent *moduli* in linear in-plane elasticity one needs at least *three* tests to determine six unknowns: C_{1111}, C_{2222}, C_{1212}, C_{1122}, C_{2211}, C_{1211} under KUBC and S_{1111}, S_{2222}, S_{1212}, S_{1122}, S_{2211}, S_{1211} under SUBC [17]. Therefore, it is interesting to find that the convergence rates in both cases are similar, which means that both methods can be equally used in estimation of the RVE.

Another distinct feature of nonlinear elasticity is the dependence of the convergence rate on deformation. We investigate such a dependence on the example of the nonlinear composite No. 1 (Figure 12). Here we define a *discrepancy* as

$$D = \frac{R^e_\delta - R^n_\delta}{\left(R^e_\delta + R^n_\delta\right)/2} \cdot 100\%, \tag{30}$$

where $R^e_\delta = \langle \Psi^e \rangle_\delta$ is the response under essential boundary conditions (KUBC) and $R^n_\delta = \langle \mathbf{P}^n : \mathbf{F}^n - \Psi^n \rangle_\delta$ is the response under natural boundary conditions (SUBC). Due to high scatter of numerical results for $\lambda \leq 1.25$, the discrepancy curve in this range is replaced by a dashed line, approaching $D = \frac{\mu^e_0 - \mu^n_0}{\left(\mu^e_0 + \mu^n_0\right)/2}$ as $\lambda \to 1$. The graph shows that the dependence of the convergence rate on the stretch value is highly nonlinear with a large difference between uniaxial and biaxial results for small λ. Moreover, the normalized *effective* response changes with the stretch ratio.

It is interesting to note that even for the neo-Hookean type composites there is a dependence of the convergence rate on the deformation. Comparing different composites at $\delta = 16$, the discrepancy is increasing in the following order: linear elastic composite, neo-Hookean composite and Ogden-neo-Hookean composite for the mismatch ratio $\alpha = 10$, and in the opposite order for the mismatch ratio $\alpha = 0.1$. The comparative study of other cases can be found in [39].

Thus, the RVE size will change depending on the quantity of interest: the maximum stretch ratio, the deformation mode and the mismatch of properties of constituents. Based on the energy bounds for composite No. 1, an approximate estimation of the RVE (under uniaxial tension, for stretch ratio $\lambda = 5$) is as follows: $\delta = 16$ corresponds to 6.4%, $\delta = 8\%$ to 11%, and $\delta = 4\%$ to 18.8% error/discrepancy in overall effective properties. Hence, if results with 6.4% accuracy are considered to be acceptable for a particular test or analysis, $\delta = 16$ can be chosen as the RVE.

3.4.2 Statistical Approach to the RVE Size Estimation

One of the methods of determination of the RVE often considered in the literature (see, for example [5, 10, 11, 18–20]), is the investigation of a property or stress/strain field fluctuation when the sample size is increased. The RVE size is then taken to be that size of the composite at which increasing the number of realizations does not improve the estimation of some particular property.

For the completeness of presentation, here, we consider such an approach and investigate the influence of the composite type and boundary conditions on the coefficient

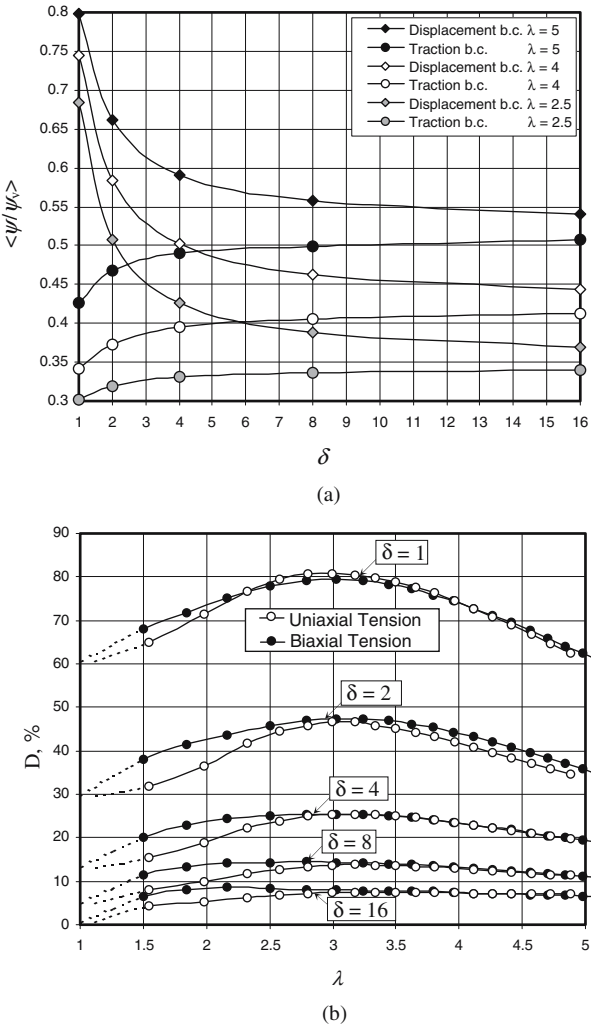

Figure 12 Discrepancies in the energy density of the composite No. 1 between displacement and traction boundary conditions for uniaxial and biaxial tension for various mesoscales.

of variation C_v of the corresponding strain energy and complementary energy (Figure 13). As can be seen from the graphs, the coefficient of variation strongly depends on boundary conditions and, with a few exceptions, is almost identical for different composites for $\delta > 8$.

For the RVE size 16 times bigger than the heterogeneity size ($\delta = 16$), the normalized standard deviation of the random fluctuations of the effective strain energy is less than 2%, whereas the discrepancy in strain energy, as it is calculated in the previous section, can be estimated to be over 6%. Thus, the statistical approach generally underestimates the size of the RVE.

4 Conclusion

In this paper we present and apply the homogenization procedure to quantitatively estimate the scale dependence of apparent responses of random composites for which the material properties of matrix and inclusion differ not only in coefficients but also in strain energy

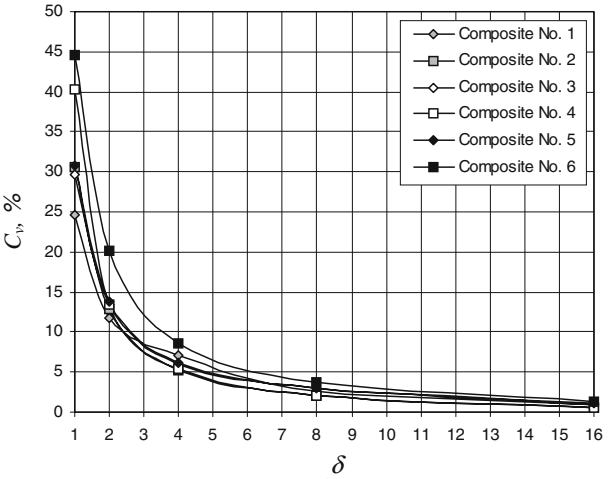

(a)

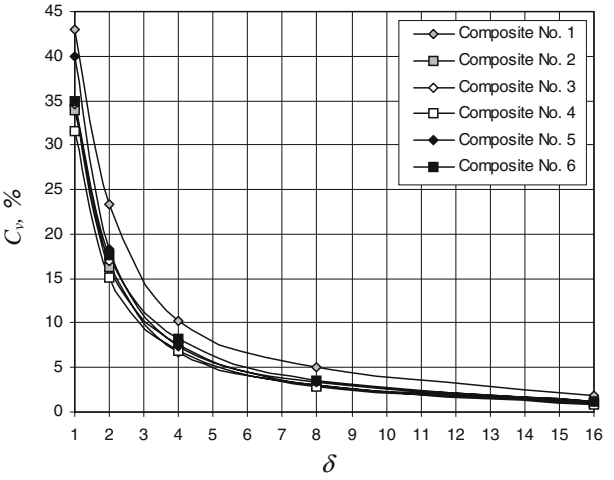

(b)

Figure 13 Dependence of the coefficient of variation of the strain energy under KUBC (a) and complementary energy under SUBC (b) on the mesoscale for different composite models.

function representations. The results obtained are compared with those where both matrix and inclusion are described by a neo-Hookean strain energy function as well as with the results of linear elasticity theory. The main findings and conclusions are summarized below:

(1) It is shown that the uniform displacement and traction boundary conditions provide, respectively, the upper and lower bounds on the stress–strain response and on the effective strain energy function for all the considered nonlinear elastic and linear elastic composites. Thus, the proposed scale-dependent homogenization allows one to estimate the RVE properties on finite scales within any desired precision.

(2) Convergence of bounds towards the RVE depends on the mismatch α, defined as the ratio between initial shear modulus of inclusions and matrix, the deformation and the deformation mode. For the mismatch ratio $\alpha = 10$ (stiff inclusions in a soft matrix) the

lower bound converges faster, whereas the mismatch ratio $\alpha = 0.1$ (soft inclusions in a stiff matrix) provides faster convergence of the upper bound.

(3) The orthogonal-mixed boundary conditions produce an intermediate response for all the considered composites.

(4) The homogenization technique, based on the investigation of the properties' fluctuations with the sample scale, provides a smaller RVE size than the technique described in the present study.

Acknowledgments The work reported herein has been made possible through support by the Werner Graupe International Fellowship, the NSERC, and the Canada Research Chairs program.

References

1. Huet, C.: Application of variational concepts to size effects in elastic heterogeneous bodies. J. Mech. Phys. Solids **38**, 813–841 (1990)
2. Sab, K.: On the homogenization and simulation of random materials. Eur. J. Mech. A, Solids **11**, 585–607 (1992)
3. Hazanov, S., Huet, C.: Order relationships for boundary conditions effect in heterogeneous bodies smaller than the representative volume. J. Mech. Phys. Solids **42**, 1995–2011 (1994)
4. Drugan, W.J., Willis, J.R.: A micromechanics-based nonlocal constitutive equation and estimates of representative volume element size for elastic composites. J. Mech. Phys. Solids **44**, 497–524 (1996)
5. Gusev, A.A.: Representative volume element size for elastic composites: a numerical study. J. Mech. Phys. Solids **45**, 1449–1459 (1997)
6. Moulinec, H., Suquet, P.: A numerical method for computing the overall response of nonlinear composites with complex microstructure. Comput. Methods Appl. Mech. Eng. **157**, 69–94 (1998)
7. Hazanov, S.: On apparent properties of nonlinear heterogeneous bodies smaller than the representative volume. Acta Mech. **134**, 123–134 (1999)
8. Michel, J.C., Moulinec, H., Suquet, P.: Effective properties of composite materials with periodic microstructure: a computational approach. Comput. Methods Appl. Mech. Eng. **172**, 109–143 (1999)
9. Drugan, W.J.: Micromechanics-based variational estimates for a higher-order nonlocal constitutive equation and optimal choice of effective moduli for elastic composites. J. Mech. Phys. Solids **48**, 1359–1387 (2000)
10. Zohdi, T.I., Wriggers, P.: On the sensitivity of homogenized material responses at infinitesimal and finite strains. Commun. Numer. Methods Eng. **16**, 657–670 (2000)
11. Zohdi, T.I., Wriggers, P.: Aspects of the computational testing of the mechanical properties of microheterogeneous material samples. Int. J. Numer. Methods Eng. **50**, 2573–2599 (2001)
12. Segurado, J., Llorka, J.: A numerical approximation to the elastic properties of sphere-reinforced composites. J. Mech. Phys. Solids **50**, 2107–2121 (2002)
13. Ren, Z.-Y., Zheng Q.-S.: Effects of grain sizes, shapes, and distribution on minimum sizes of representative volume elements of cubic polycrystals. Mech. Mater. **36**, 1217–1229 (2004)
14. Soize, C.: Random-field model for the elasticity tensor of anisotropic random media. C. R. Méc. **332**, 1007–1012 (2004)
15. Lachihab, A., Sab K.: Aggregate composites: a contact based modeling. Comp. Mat. Sci. **33**, 467–490 (2005)
16. Sab, K., Nedjar, B.: Periodization of random media and representative volume element size for linear composites. C. R. Méc. **333**, 187–195 (2005)
17. Ostoja-Starzewski, M.: Material spatial randomness: from statistical to representative volume element. Probab. Eng. Mech. **21**, 112–132 (2006)
18. Löhnert, S., Wriggers, P.: Homogenization of microheterogeneous materials considering interfacial delamination at finite strains. Tech. Mech. **23**, 167–177 (2003)
19. Löhnert, S.: Computational homogenization of microheterogeneous materials at finite strains including damage. Dissertation, Hannover University (2004)
20. Hohe, J., Becker, W.: A probabilistic approach to the numerical homogenization of irregular solid foams in the finite strain regime. Int. J. Solids Struct. **42**, 3549–3569 (2005)

21. Kouznetsova, V., Geers, M.G.D., Brekelmans, W.A.M.: Size of a representative volume element in a second-order computational homogenization framework. Int. J. Mult. Comp. Eng. **2**, 575–598 (2004)
22. Ostoja-Starzewski, M.: Scale effects in plasticity of random media: status and challenges. Int. J. Plast. **21**, 1119–1160 (2005)
23. Khisaeva, Z.F., Ostoja-Starzewski, M.: Mesoscale bounds in finite elasticity of random composites. Proc. R. Soc. Lond. A **462**, 1167–1180 (2006)
24. Torquato, S.: Random Heterogeneous Materials. Microstructure and Macroscopic Properties. Springer, Berlin Heidelberg New York (2002)
25. Hill, R.: On constitutive macro-variables for heterogeneous solids at finite strain. Proc. R. Soc. Lond. A **326**, 131–147 (1972)
26. Nemat-Nasser, S.: Averaging theorems in finite deformation plasticity. Mech. Mater. **31**, 493–523 (1999)
27. Lee, S.J., Shield, R.T.: Variational principles in finite elastostatics. J. Appl. Math. Phys. (ZAMP) **31**, 437–453 (1980)
28. Ogden, R.W.: Extremum principles in nonlinear elasticity and their application to composites – I. Int. J. Solids Struct. **14**, 265–282 (1978)
29. Ponte Castañeda, P.: The overall constitutive behavior of nonlinearly elastic composites. Proc. R. Soc. Lond. A **422**, 147–171 (1989)
30. Hashin, Z., Shtrikman, S.: A variational approach to the theory of the elastic behaviour of multiphase materials. J. Mech. Phys. Solids **11**, 127–140 (1963)
31. Gatos, K.G., Thomann, R., Karger-Kocsis, J.K.: Characteristics of ethylene propylene diene monomer rubber/organoclay nanocomposites resulting from different processing conditions and formulations. Polym. Int. **53**, 1191–1197 (2004)
32. Martin, P., Maquet, C., Legras, R., Bailly, C., Leemans, L., van Gurp, M., van Duin, M.: Particle-in-particle morphology in reactively compatibilized poly(butylene terephthalate)/epoxide-containing rubber blends. Polymer **45**, 3277–3284 (2004)
33. Wong, S.C., Mai, Y.W.: Effect of rubber functionality on microstructures and fracture toughness of impact-modified nylon 6,6/polypropylene blends. 1. Structure–property relationships. Polymer **40**, 1553–1566 (1999)
34. Schneider, M., Pith, T., Lambla, M.: Toughening of polystyrene by natural rubber-based composite particles. J. Mater. Sci. **32**, 6331–6342 (1997)
35. Brain network laboratory. Texas A&M University, Texas. http://research.cs.tamu.edu/bnl/galleryData.html. Cited 3 Apr (2006)
36. Ogden, R.W.: Non-Linear Elastic Deformations. Halsted, New York (1984)
37. Rivlin, R.S.: Large elastic deformations of isotropic materials. I. Fundamental concepts. Phil. Trans. Roy. Soc. A **240**, 459–490 (1948)
38. Ogden, R.W., Saccomandi, G., Sgura, I.: Fitting hyperelastic models to experimental data. Comput. Mech. **34**, 484–501 (2004)
39. Ostoja-Starzewski, M., Du, X., Khisaeva, Z.F., Li, W.: On the size of representative volume element in elastic, plastic, thermoelastic and permeable random microstructures. Keynote lecture in Thermec'2006, Int. Conf. Processing & Manufacturing Adv. Mater., Vancouver, Canada.